Optoelectronic switches based on wide bandgap semiconductors

ARTICLE *in* THE JOURNAL OF PHYSICAL CHEMISTRY B · JANUARY 2006

Impact Factor: 3.3

4 AUTHORS, INCLUDING:

Konrad Szacilowski
AGH University of Science and Technology …
87 PUBLICATIONS **1,848** CITATIONS
SEE PROFILE

Wojciech Macyk
Jagiellonian University
88 PUBLICATIONS **2,074** CITATIONS
SEE PROFILE

JPCBFK

VOLUME 110
AUGUST 10, 2006
NUMBER 31

http://pubs.acs.org/JPCB

THE JOURNAL OF PHYSICAL CHEMISTRY B

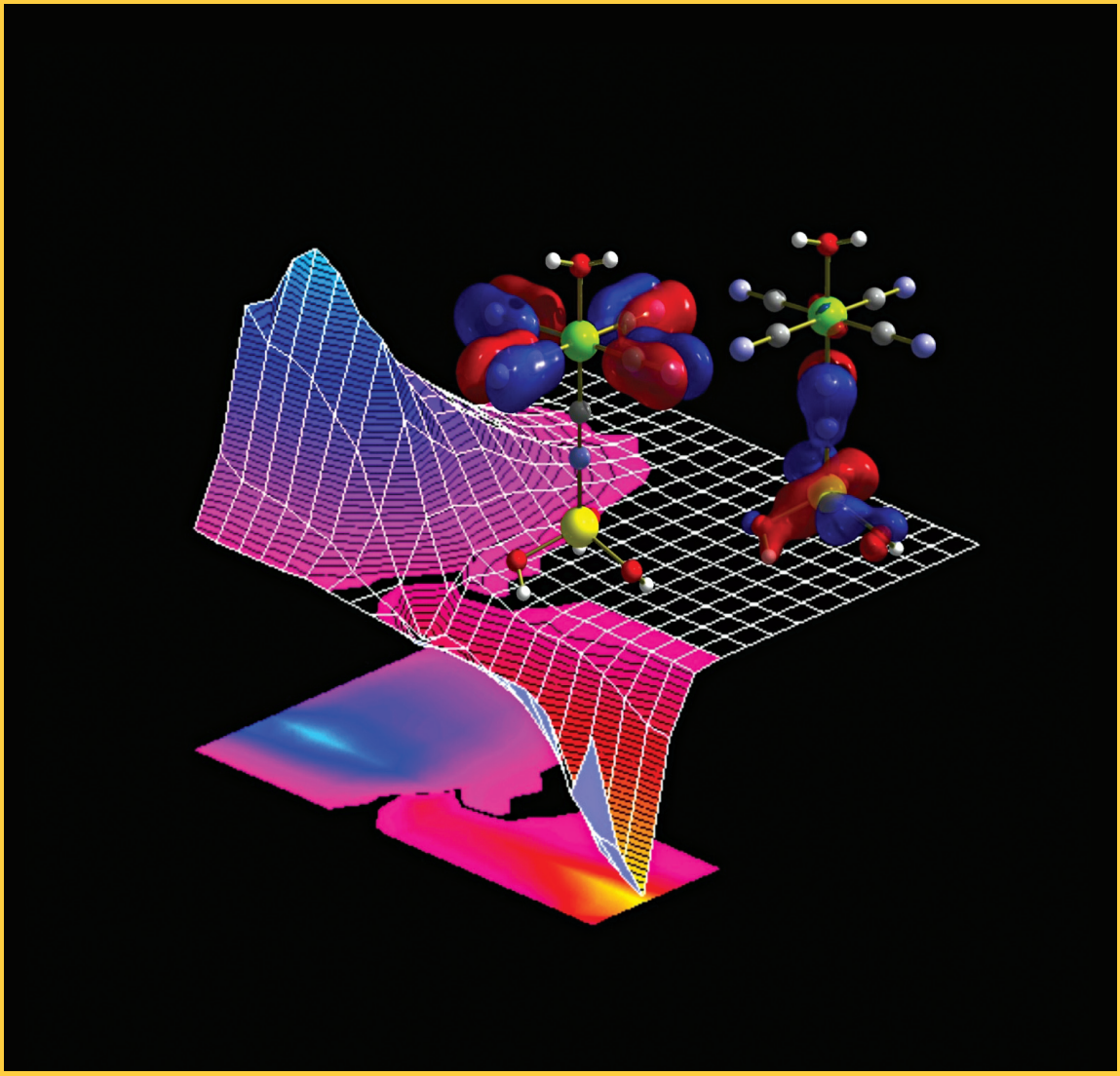

Photocurrent Dependence on Potential and Incident Light Wavelength Photogenerated at Titania Modified with Cyanoferrate Complexes
(see page 15275)

CONDENSED MATTER, MATERIALS, SURFACES, INTERFACES, & BIOPHYSICAL CHEMISTRY

PUBLISHED WEEKLY BY THE AMERICAN CHEMICAL SOCIETY

Optoelectronic Switches Based on Wide Band Gap Semiconductors

Maciej Hebda, Grażyna Stochel, Konrad Szaciłowski,* and Wojciech Macyk*

Faculty of Chemistry, Jagiellonian University, Ingardena 3, 30-060 Kraków, Poland

Received: February 28, 2006; In Final Form: April 24, 2006

Switching of photocurrent direction in semiconducting systems upon changes of the electrode potential or incident light wavelength was realized by a series of photoelectrodes covered with titania modified with pentacyanoferrate complexes, $[Fe(CN)_5L]^{n-}$ (L = NH_3, thiodiethanol, thiodipropanol). These materials were characterized by optical spectroscopy and electrochemistry. The structure of the surface complexes was modeled using simple quantum-chemical models. The electrodes described in this paper enable control of the photocurrent direction by two stimuli: Changing the wavelength or the photoelectrode potential easily switches the direction of photocurrent. The materials are different from those of similar characteristics studied by other authors: They are not composites comprising of two types of semiconductors but rather engineered uniform materials. The photocurrent switching phenomenon is an intrinsic feature resulting from a specific electronic structure of the surface-modified semiconductor.

1. Introduction

Wide band gap nanocrystalline semiconductors have found numerous applications as (photo)catalysts,[1,2] chemosensors, and biomimetic light-harvesting antennae.[3−5] Surface modification of these materials results in significant improvement of their properties. The most important modification consists of photosensitization of wide band gap semiconductors toward visible light.[5] These materials, due to their unique optical and photoelectric properties, have found applications in dye-sensitized solar cells,[6−9] optical or photoelectrochemical sensors,[10,11] and photocatalysts.[1,2,9,12−15] The materials formed via chemisorption of various transition metal complexes or organic dyes on surfaces of mesoporous and nanocrystalline wide band gap semiconductors are used as active components of solar cells. The surface complex usually plays the role of light-harvesting antenna, while the semiconducting structure acts as the charge separation device and provides mechanical support of the photosensitizer.[5,6,16]

Also systems attached to the surface of titania acting as molecular switches were recently described.[17−19] The increasing interest in molecular electronics stimulated research on switching properties of some semiconductor composite materials of prospective importance for optoelectronics and sensor engineering.

The phenomenon of photocurrent switching has been described recently for hydrogen-modified amorphous SiC wafers containing stacked p−i−n heterojunctions.[20−22] These devices generate photocurrent whose direction and intensity depends on bias potential and incident light wavelength. The process of tuning the spectral sensitivity[23] of these devices is used for construction of image and color sensors and pattern-recognition instruments.[24,25] Quite similar effects have been observed in photoelectrodes prepared from $[Fe(CN)_6]^{4-}$-modified titania.[26−28]

This article describes in detail the photoelectrochemical properties of surface-modified titanium dioxide with chemisorbed pentacyanoferrate complexes of the $[Fe(CN)_5L]^{n-}$ type. Upon irradiation these materials generate anodic and cathodic photocurrents depending on the applied electrode potential, wavelength of incident light, presence of oxygen, and ligand L structure.

Pentacyanoferrates are versatile complexes with easily tunable redox and optical properties. Various C-, N-, S-, and P-donors are relatively strongly bound to the iron center.[29−31] Complexes with soft ligands (cyanide, thioethers, phosphines) seem to be especially suited for photoelectrochemical investigations due to their stability and reversibility of electrode processes.[31−34] They can be easily synthesized in ligand substitution reactions from $[Fe(CN)_5NH_3]^{3-}$ or $[Fe(CN)_5H_2O]^{3-}$ complexes. In addition, various cyanoferrate complexes undergo facile chemisorption at surfaces of nanocrystalline semiconductors.[26,27,35−39] These surface adducts usually show metal-to-metal charge transfer (MMCT; $Fe^{II} \rightarrow Ti^{IV}$) transitions in the visible range of the electromagnetic spectrum making them suitable for modification of optical and electronic properties of titania and other semiconducting materials.

2. Experimental Methods

2.1. Materials. TiO_2 (Degussa P25, ca. 70% anatase, 30% rutile; 50 $m^2\ g^{-1}$) was used to prepare porous electrodes. The indium tin oxide (ITO) slides (∼2 cm^2, Aldrich) were etched for at least 12 h in 15% NaOH solution, washed with distilled water, and air-dried. A small sample of TiO_2 powder was suspended in distilled water and cast onto the cleaned surface of an ITO slide. After being dried in hot air copper wire was attached to the ITO surface using silver glue, and the whole junction area was insulated with water-resistant self-adhesive insulation tape. The electrodes were modified in 0.01 M aqueous solutions of $Na_3[Fe(CN)_5NH_3]\cdot 3H_2O$ (prepared according to Brauer),[40] containing, if desired, a 10-fold excess of the thioether ligand. Thioethers insoluble in water were dissolved in 90% ethanol, and the resulting solutions were mixed with an aqueous solution of the $Na_3[Fe(CN)_5NH_3]$ complex. The mixtures were heated gently to 80 °C for 5 min. Small amounts of unreacted insoluble thioethers were filtered off using syringe filters. After 10 min electrodes were carefully washed with distilled water

* Authors to whom correspondence should be addressed. Phone: +48 12 663 2208 (K.S.); +48 12 663 2005 (W.M.). Fax: +48 12 634 0515. E-mail: szacilow@chemia.uj.edu.pl; macyk@chemia.uj.edu.pl.

10.1021/jp061262b CCC: $33.50
Published on Web 06/15/2006

and used immediately for measurements. Thioethers and dimethyl sulfoxide (DMSO) were purchased from Aldrich and used as received.

Titanium dioxide nanoparticles were synthesized from hydrolyzed isopropyl orthotitanate. A mixture prepared from 2.5 cm^3 of titanate ester and 45 cm^3 of isopropyl alcohol was added dropwise to 450 cm^3 of vigorously stirred water acidified with concentrated nitric acid to pH = 1 at 1 °C. The whitish colloidal solution was stirred overnight in an ice bath yielding an almost transparent solution of TiO_2 nanoparticles.

2.2. Instrumentation. The typical three-electrode setup was employed for photoelectrochemical measurements. The electrolyte solution was 0.1 M KNO_3, which was kept in equilibrium with air or was purged with argon for at least 15 min prior to the measurement. Platinum and Ag/AgCl were used as the auxiliary and reference electrodes, respectively. A 150 W XBO lamp (Osram) equipped with a water-cooled housing and LPS 200 power supply (Photon Technology International) was used for irradiation. The working electrodes were irradiated from the backside (through the ITO glass) to minimize the influence of the thickness of the semiconductor layer on the photocurrent. An automatically controlled monochromator and a shutter were applied to choose the appropriate energy of radiation. Dark electrochemical measurements were performed using platinum and vitreous carbon electrodes. The electrochemical measurements (CV, CV + chopped light, photocurrent action spectra) were controlled by BAS 50W (Bioanalytical Instruments, USA) or M161 (MTM, Poland) electrochemical analyzers. Photocurrent action spectra were not corrected for light intensity. Absorption spectra were recorded in 1 cm path length optical cells on a HP 8453 diode array spectrophotometer. Diffuse reflectance spectra were recorded on a Perkin-Elmer Lambda 35 spectrophotometer equipped with a 5 cm diameter integrating sphere. Magnesium oxide was used as a reference material.

2.3. Calculations. Theoretical modeling was performed with ArgusLab 4.0.1 (Planaria Software, USA).[41] Geometry was optimized with the molecular mechanics module[42−45] using the UFF force field,[46−49] while frontier orbital contours were obtained using the ZINDO[50] semiempirical method.

The electric circuit shown in Figure 11 was numerically modeled using the Spice/XSpice simulator CircuitMaker 6.2 (Protel Technology, Inc., USA). The R_1 and R_3 resistances were set equal 10 kΩ, the R_2 resistance was set equal 100 kΩ, $R_{ITO} + R_e + R_{load}$ also was equal to 10 kΩ, and the inner source resistance $R_s = 500$ Ω.[51,52] The capacitances of the C_1 and C_3 capacitors were experimentally adjusted to 50 and 10 μF, respectively. The capacitance C_2 was varied within 0.001−1000 μF. The voltage supply was a square wave generator of the following characteristics: initial potential 0 V, peak amplitude 5 V, pulse period 5 s, pulse width 2.5 s, pulse rise time 1 ns, pulse fall time 1 ns.

3. Results

3.1. Structure, Bonding, and Redox Properties. Amminepentacyanoferrate(II) easily hydrolyzes in aqueous solutions[53] (eq 1) and reacts with thioethers (R_2S) and sulfoxides (R_2SO) yielding stable thioether and sulfoxide complexes, respectively (eq 2)[31−33,54−56]

$$[Fe^{II}(CN)_5NH_3]^{3-} + H_2O \rightleftarrows [Fe^{II}(CN)_5H_2O]^{3-} + NH_3 \quad (1)$$

$$[Fe^{II}(CN)_5L]^{3-} + L' \rightleftarrows [Fe^{II}(CN)_5L']^{3-} + L \quad (2)$$

$$(L = NH_3, H_2O; L' = R_2S, R_2SO)$$

TABLE 1: Redox Potentials for Various $[Fe^{III/II}(CN)_5L]^{n-}$ Couples vs the Ag/AgCl Reference Electrode Obtained from Cyclic Voltammetry Measurements

ligand	$E_{1/2}{}^a$ (mV)	$E_{1/2}{}^b$ (mV)
CN^-	259	299
NH_3	119	240
1,3-dithiane	240	378
2,2′-thiodiethanol (tde)	257	281
1,3-dithiolane	273	*c*
methionine	302	392
3,3′-thiodipropanol (tdp)	306	345
3,3′-thiodipropionate	327	371
3,3′-thiodipropionitril	397	374
2,2′-thiodiacetate	405	410
dimethyl sulfoxide (DMSO)	559	*c*

[a] In solution. [b] On the TiO_2 surface. [c] Does not chemisorb efficiently on the TiO_2 electrodes.

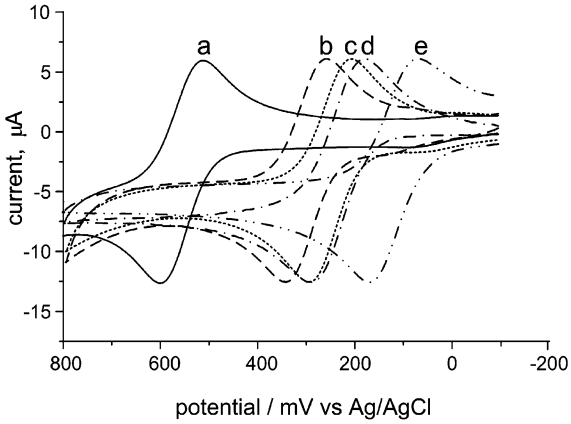

Figure 1. Cyclic voltammograms of the studied cyanoferrates: $[Fe(CN)_5DMSO]^{3-}$ (a), $[Fe(CN)_5tdp]^{3-}$ (b), $[Fe(CN)_5tde]^{3-}$ (c), $[Fe(CN)_6]^{4-}$ (d), and $[Fe(CN)_5NH_3]^{3-}$ (e).

Thioether and DMSO complexes undergo a reversible one-electron oxidation at potentials more positive than the parent complex (Table 1). The redox potentials of thioether complexes usually fall within the 240−405 mV range, and the DMSO complex shows a reversible one-electron reduction at +559 mV vs Ag/AgCl, while the parent ammine complex shows a one-electron reversible wave at +119 mV (Figure 1). All studied compounds show relatively strong metal-centered (MC) transitions[33,54,57] within 350−400 nm (Figure 2a). In contrary to aromatic amine complexes, the $[Fe^{II}(CN)_5SR_2]^{3-}$ species do not exhibit any metal-to-ligand charge transfer MLCT transitions within 300−1100 nm.

Pentacyanoferrates(II) are easily adsorbed onto the TiO_2 surface. The binding to the surface, as in the case of the $[Fe(CN)_6]^{4-}$ complex,[58] should involve formation of Ti−N≡C−Fe bridges (Figure 3a), but no detailed spectroscopic or photoelectrochemical characteristics on these materials are available. They are characterized by a broad MMCT absorption band in the visible range (Figure 2c). The same absorption bands are observed upon mixing aqueous solutions of pentacyanoferrates with colloidal solutions of titania nanocrystals (Figure 2b). In both cases the MMCT bands are broad and extend from ∼350 to 600−650 nm, except that of the DMSO complex, which exhibits only a very weak sensitization toward visible light. Simple quantum-chemical calculations indicate that the most probable binding via the axial cyanide ligand takes place, which is also the most probable binding mode from a purely geometrical point of view, especially in the case of a bulky sixth ligand.

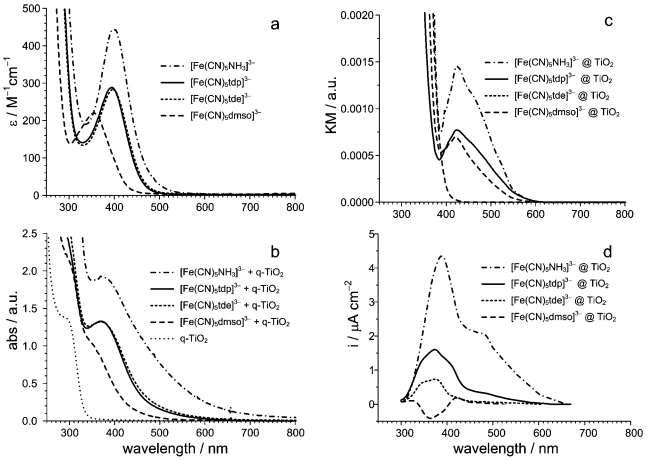

Figure 2. Absorption spectra of the studied pentacyanoferrates in neat aqueous solutions (a), absorption spectra of the same complexes in the presence of TiO_2 nanoparticles (b), diffuse reflectance spectra of cyanoferrate complexes chemisorbed on nanocrystalline titania (c), and photocurrent action spectra recorded at −150 mV vs Ag/AgCl.

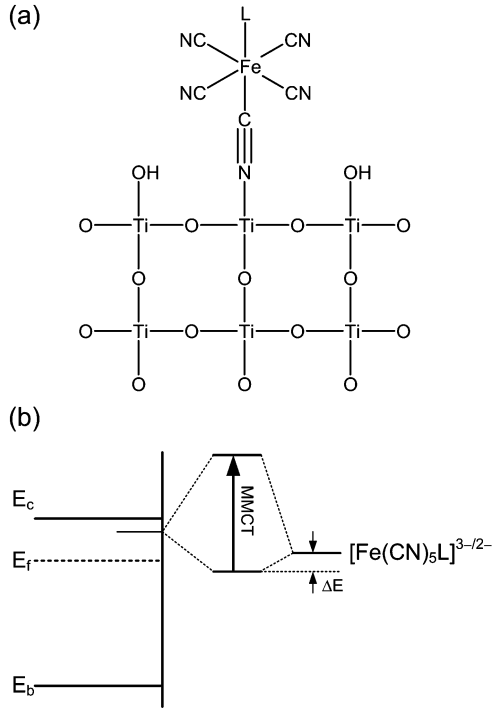

Figure 3. Scheme of the surface complex formation between penta- ($L \neq CN^-$) and hexacyanoferrates and titanium dioxide: the simplified structure of the surface complex (a) and the energy diagram (b).

The reaction of pentacyanoferrates with the surface of titanium dioxide crystals (containing Ti−OH centers) can be regarded as a nucleophilic substitution reaction, with titanium ions playing the role of central ions and cyanoferrate anions acting as ligands. Therefore the reactivity of the cyanoferrate complexes depends to a large extent on the properties of the highest occupied molecular orbitals (HOMOs) of the nucleophile and the lowest unoccupied molecular orbitals (LUMOs) of the electrophile. Empty band gap states between the lower edge of the conduction band and the Fermi level are the most probable electrophilic sites for this reaction (Figure 3b).[11] According to simple ZINDO calculations the HOMOs of the $[Fe(CN)_5NH_3]^{3-}$, $[Fe(CN)_5H_2O]^{3-}$, $[Fe(CN)_5tde]^{3-}$, and $[Fe(CN)_5tdp]^{3-}$ anions are localized mainly on the carbon and nitrogen atoms of the axial cyanide ligands with significant contributions from the d-orbitals of the central iron ion (Figure 4). This electronic configuration not only ensures strong binding of the complex to the TiO_2 surface but also provides a platform for an efficient photoinduced electron transfer between Fe^{II} and Ti^{IV} centers. The efficient bonding between $[Fe(CN)_5L]^{3-}$ anions and Ti^{IV} oxo-species was substantiated in a simple model system $[Fe(CN)_4(H_2O)-C\equiv N-Ti(OH)_3]^{2-}$, where the TiO_2 surface is simplified to one titanium(IV) ion with three hydroxide ligands (Figure 5). The HOMO of this species is localized mainly on the equatorial cyanide ligands and iron ion, while the LUMO is localized on the bridging cyanide ligand and the titanium(IV) ion. It proves that the low-energy transition (HOMO → LUMO) in this complex includes electron transfer from the cyanoferrate moiety toward the titanium center. Similar results were recently reported for $[Fe(CN)_6]^{4-}$ bound to the TiO_2 nanocluster.[58]

Bonding of the cyanoferrate moieties to the surface of titanium dioxide results in a significant decrease of the HOMO energy, which is manifested by increasing the oxidation potential of the bound $[Fe(CN)_5L]^{3-}$ with respect to the same anion in solution (Figure 3b, cf. Table 1). Electrochemical investigation of the surface-bound pentacyanoferrates indicates that the strongest interaction occurs between titanium dioxide and the $[Fe(CN)_5(1,3\text{-dithiane})]^{3-}$ complex, and the increase of redox potential amounts to 138 mV, while for other studied complexes it amounts to 24−121 mV, cf. ΔE in Figure 3b. Complexes containing thioether ligands with electron-withdrawing groups in the vicinity of the binding site show only a very small increase (2,2′-thiodiacetate, 5 mV) or small decrease (3,3′-thiodipropionitrile, −23 mV) of the redox potential. A strong interaction between pentacyanoferrate complexes and the semiconductor support is reflected in exceptionally efficient sensitization of TiO_2 toward visible light by the $[Fe(CN)_5NH_3]^{3-}$ complex (Figure 2d). This tendency also can be seen when various pentacyanoferrates are deposited on TiO_2 nanocrystalline suspensions (cf. Figure 2b). UV−visible spectra indicate the formation of new absorption bands due to MMCT ($Fe^{II} \rightarrow Ti^{IV}$) transitions. The $[Fe(CN)_5NH_3]^{3-}$ complex shows the most intense and the broadest MMCT transition, which is in agreement with electrochemical data on surface-bound complexes.

Most of the thioether complexes, although stable in solution, are relatively unstable when bound to the surface of titanium dioxide. On electrochemical oxidation they tend to desorb from the surface or substitute the thioether ligand with a water molecule. This effect is associated with the decreased stability of the Fe−S bond for Fe^{III} as compared with that for Fe^{II} complexes, already observed for thiocarbonyl ligands.[34] Only the pentacyanoferrate complexes with ammonia, thiodiethanol, and thiodipropanol show sufficient stability for photoelectrochemical studies. Photoelectrodes comprised of cyanoferrate-modified nanocrystalline titanium dioxide resist at least 1000 switching cycles without any changes in photoelectrochemical characteristics (vide infra).

3.2. Photoelectrochemistry. Photocurrent generation by transparent ITO electrodes covered with $[Fe(CN)_5L]^{n-}@TiO_2$ was investigated in two modes—as a function of the electrode potential and incident light wavelength.

A typical example of a voltammogram recorded upon chopped monochromatic light irradiation ($\lambda = 350$ nm) is shown in Figure 6. Depending on the accessibility of an electron acceptor in the electrolyte solution (in this case oxygen) the photocurrent generation at a $[Fe(CN)_5L]^{n-}@TiO_2$ electrode follows two different behaviors:

In the presence of oxygen the anodic photocurrent was recorded at potentials higher than the potential of the redox wave

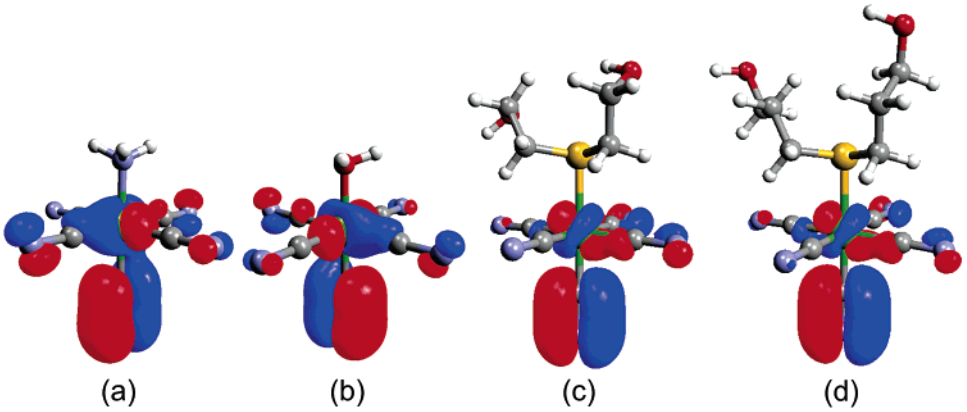

Figure 4. MM/UFF-optimized geometries and contours of the HOMOs of the $[Fe(CN)_5NH_3]^{3-}$ (a), $[Fe(CN)_5H_2O]^{3-}$ (b), $[Fe(CN)_5tde]^{3-}$ (c), and $[Fe(CN)_5tdp]^{3-}$ (d) anions as calculated using the ZINDO method.

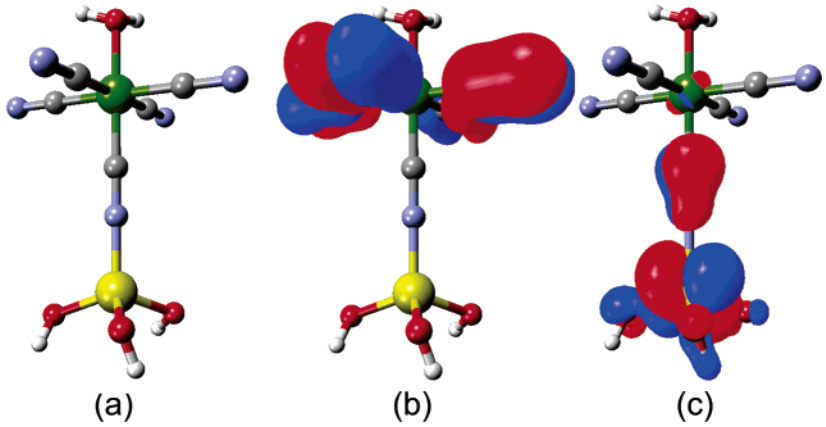

Figure 5. MM/UFF-optimized structure of the model complex $[Fe(CN)_4(H_2O)-C\equiv N-Ti(OH)_3]^{2-}$ (a) and its HOMO (b) and LUMO (c).

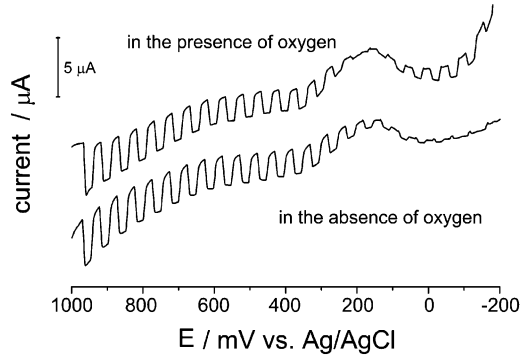

Figure 6. Current vs potential diagrams recorded for $[Fe(CN)_6]^{4-}$@TiO_2 in the presence and absence of oxygen. Conditions: scan rate 10 mV s^{-1}, chopped light 350 nm.

associated with the oxidation/reduction of the surface complex. In the range of potentials where the reduced form of the complex is present the photocurrent direction is opposite. The photocurrent switching point is closely related to the potentials of quasi-reversible waves of surface $[Fe(CN)_5L]^{n-}$ complexes (Figure 6).

In the absence of oxygen generation of anodic photocurrents resembles the situation described above. However, in this case no switching point appears. In the presence of the reduced form of the surface complex no cathodic photocurrents but only residual anodic signals were recorded (Figure 6).

Photocurrent measurements as a function of incident light wavelength also show a switching behavior in a certain range of applied potentials close to the redox potential of the surface complex (Figure 7). Also in this case the influence of oxygen was tested, as demonstrated for $[Fe(CN)_5tdp]^{3-}$@TiO_2. Values

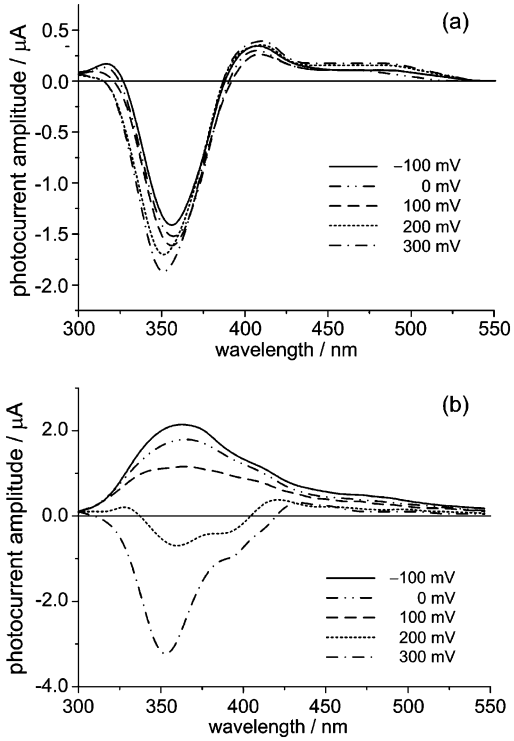

Figure 7. Photocurrent action spectra recorded for the $[Fe(CN)_5tdp]^{3-}$-modified titanium dioxide at various photoelectrode potentials in the absence (a) and in the presence (b) of molecular oxygen.

of the photocurrent have been read as a difference between the steady-state current measured upon irradiation and the current in the dark just before opening the shutter. A significant effect

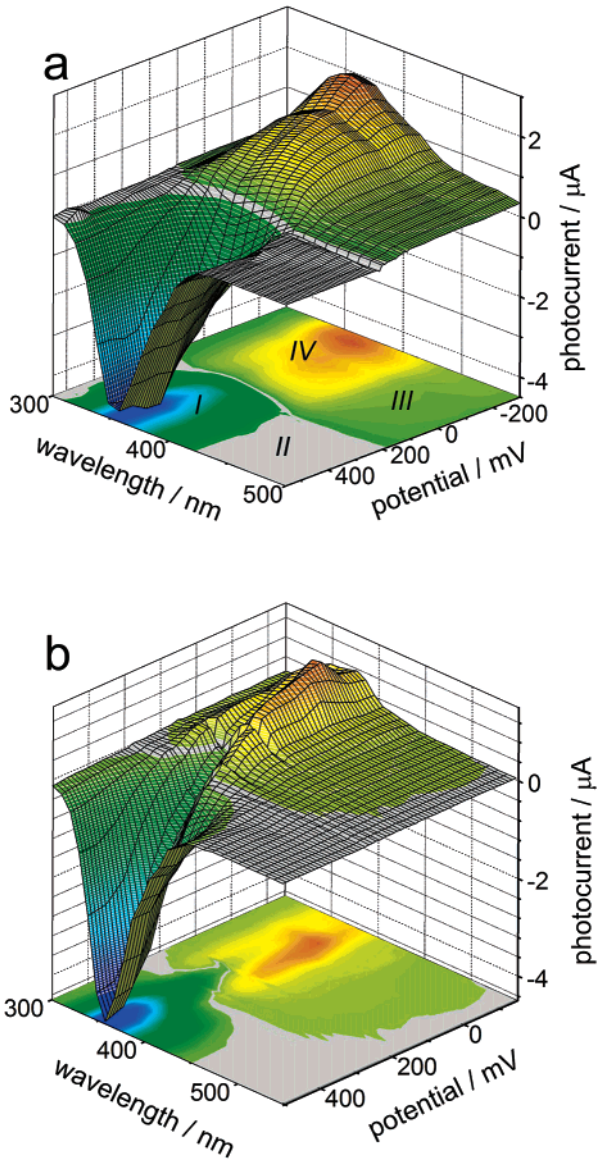

Figure 8. Photocurrents generated at $[Fe(CN)_5tdp]^{3-}$ (a) and $[Fe(CN)_5tde]^{3-}$ (b) modified titanium dioxide photoelectrodes as a function of electrode potential and incident light wavelength.

of oxygen can be seen at potentials lower than the reduction potential of the surface complex. In the absence of O_2 only slight differences in $I_{ph}(\lambda)$ are observed when the photoelectrode potential is shifted in the cathodic direction (Figure 7a). The situation changes dramatically when O_2 is present (Figure 7b). Anodic photocurrents recorded at positive potentials upon UV irradiation decrease to become cathodic at more negative E values. In the visible range of incident light cathodic photocurrents increase with decreasing potential.

To have a full overview of photocurrent generation as a function of applied potential and irradiation wavelength a set of action spectra was collected at constant potentials (at every 25 mV). In this way three-dimensional (3D) pictures (phase diagrams or maps) were obtained (Figure 8). Photocurrent values used for the map construction are not corrected for changes in incident light intensities with irradiation wavelength.

3.3. The Switching Mechanism. The possibility of anodic and cathodic photocurrent generation depends on the oxidation state of the surface cyanoferrate complex. The results presented above confirm this observation—the potential at which the photocurrent direction changes correlates very well with the redox potential of the complex chemisorbed at the titania surface. At potentials more positive as compared to $E_{1/2}$ of the cyanoferrate complex excitation of the surface iron(III) species does not lead to electron injection into the conduction band. Under such conditions only excitation of the semiconductor matrix may result in photocurrent generation. In analogy to the unmodified n-type semiconductor (Figure 9a) the anodic photocurrents can be observed (Figure 9b).

Even partial reduction of the surface complex opens the possibility of cathodic photocurrent generation (Figure 9c). Excitation of the iron(II) surface complex gives an electron in the conduction band or excited states of the surface complex. The cathodic photocurrent appears as a result of the electron transfer from the electrode (ITO or metal) to the partially emptied bonding orbital of the surface complex of the semiconductor and from the conduction band to solution. This mechanism assumes the presence of an efficient electron acceptor in solution. A good candidate for the electron acceptor is an oxygen molecule ($E_{O_2/O_2^-} = -0.16$ V vs the normal hydrogen electrode).[59,60] To prove the role of oxygen photocurrent generation in the presence and absence of O_2 was compared (Figure 6). The lack of an electron scavenger causes no cathodic photocurrents to be observed.

A good example demonstrating which type of photocurrent generation mechanism prevails is a 3D map recorded for $[Fe(CN)_5tdp]^{n-}@TiO_2$ (Figure 8a) in the presence of oxygen. In this case four main different regions can be considered: (i) potentials higher than $E_{1/2}$ and UV light irradiation, (ii) potentials higher than $E_{1/2}$ and visible light irradiation, (iii) potentials lower than $E_{1/2}$ and visible light irradiation, and (iv) potentials lower than $E_{1/2}$ and UV irradiation. In area i the mechanism shown in Figure 9b is dominant due to direct excitation of titania. There is no photocurrent response in area ii since the photon energy is too low to excite TiO_2 while light absorption by the surface

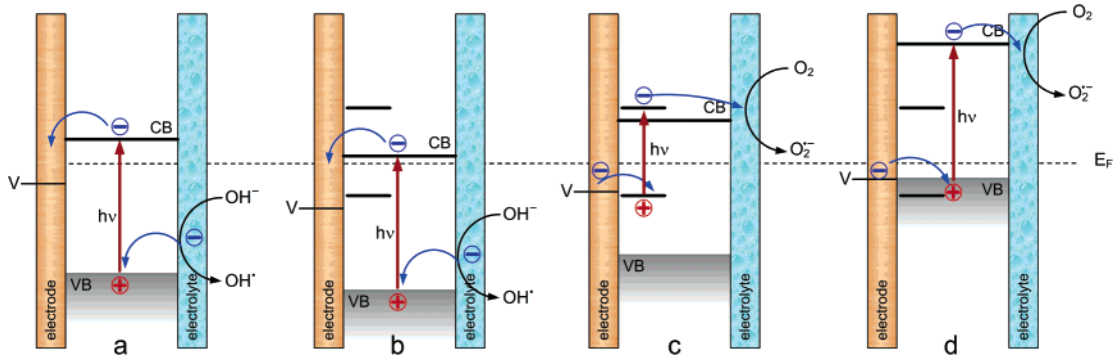

Figure 9. Mechanism of photocurrent generation (the PEPS effect). Anodic photocurrent is generated at neat TiO_2 (a) and TiO_2 with an oxidized surface complex (b), while cathodic photocurrents appear after partial reduction of the surface complex (c) and under inversion layer conditions (d).

iron(III) complex cannot result in electron excitation to the conduction band of the semiconductor. The mechanism shown in Figure 9c prevails in area iii because visible light absorption by the reduced surface complex (within the MMCT band) results in electron injection into the conduction band of titania. Under these conditions titanium dioxide is photosensitized to visible light. Finally, conditions in area iv allow for the mechanism shown in Figure 9d.

This description, however, does not explain the more subtle shapes of recorded maps. To understand why switching points move by tenths of nanometers with the changing electrode potential the geometric factors should be considered.[26,27] The depth of photon penetration depends on the photon energy and absorption spectrum of the material. Irradiation within the MMCT absorption band of the surface complex does not affect the inner part of the semiconductor particle, and only the electron transfer processes presented in Figure 8c may take place (cathodic photocurrent). The surface layer may be transparent for photons of higher energy, which are absorbed by the nearly unmodified core of the semiconductor particle. The inner part of the material grain is responsible rather for the anodic photocurrent, and therefore at shorter wavelengths this effect is observed. Subtle changes of the photoelectrode potential close to the $E_{1/2}$ value enable control of the ratio between the reduced and the oxidized forms of the surface complex. Increasing the amount of the reduced pentacyanoferrate surface species by lowering the photoelectrode potential facilitates generation of higher cathodic currents. At these potentials decreasing anodic photocurrents generated according to the mechanism presented in Figure 9b compete with increasing cathodic photocurrents generated as shown in Figure 9c. The net current may be anodic or cathodic depending on values of component photocurrents and therefore also on incident light wavelength. This explains the photocurrent switching by changing the energy of applied photons. Such an effect can be easily observed for the $[Fe(CN)_5tde]^{n-}@TiO_2$ photoelectrode (Figure 8b) in the presence of oxygen in the potential range of ca. 150−300 mV vs Ag/AgCl. The effect of photocurrent direction switching induced by changes of the electrode potential or the wavelength of incident light is called photoelectrochemical photocurrent switching (PEPS).[26,28]

3.4. Kinetic Analysis and Modeling. The kinetic traces of photocurrent generated upon pulsed irradiation can give some insight into electric properties of the semiconducting photoelectrodes.[51] Depending on the photoelectrode potential and incident light wavelength the photoelectrical response of the electrode varies significantly. The main and most evident change is of course the photocurrent direction as discussed in the preceding section of this paper. Apart from that there are two distinct types of kinetic responses. The first one, observed mostly in the UV range at high electrode potentials (in the anodic range of parameters), shows a rapid increase of the photocurrent upon shutter opening until the steady-state value; when the shutter is subsequently closed, photocurrent decays in the second time scale to the background value (Figure 10a). The second limiting case shows an immediate increase of the photocurrent upon shutter opening and a subsequent slow decrease to the steady-state photocurrent. When the shutter is closed, the photocurrent immediately changes its direction and then slowly decays to the background value. This kinetic trace shows two sharp spikes: upon shutter opening and closure (Figure 10b). Another characteristic behavior is observed when the applied parameters approach the photocurrent switching region: The photocurrent profiles show at the same time charging−discharging character

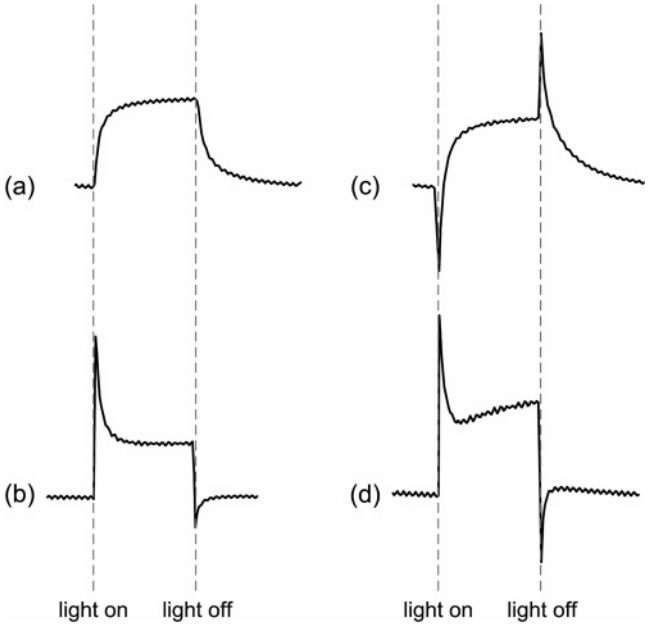

Figure 10. "Pure" photocurrent kinetic profiles: charge−discharge curves, characteristic for anodic photocurrents (a); spiked, characteristic for cathodic photocurrents (b). Mixed photocurrent kinetic profiles: anodic charge−discharge profile with spiked contribution of cathodic response (c); spiked cathodic pulse with contribution of charge−discharge component (d).

and sharp spikes at points of shutter opening and closure (Figures 10c and 10d). This behavior is characteristic for both anodic and cathodic photocurrents. Cathodic spikes may originate from reduction of species absorbed on the semiconductor surface by electrons from the conduction band, while anodic peaks are the result of oxidation of surface species by holes from the valence band. This explains why the spiked photocurrent profiles are observed mainly near the redox potential of the surface cyanoferrate: At this potential range both the oxidized and the reduced form of the complex are available for this type of reaction.

This complex behavior implies that the semiconducting photoelectrode composed of surface-modified titania is a complex electric system. To describe the electrode properly one must take into account its complex structure. The electrode consists of semiconducting powder deposited on the surface of ITO glass immersed in electrolyte solution. The layer of semiconductor particles in not compact, so electrolyte can easily permeate the porous semiconducting film. Therefore one can treat the electrode as a system consisting of a conductor−semiconductor junction (Schottky rather than Ohmic)[61,62] and Helmholtz double layer connected in series.[63] In addition an RC circuit mimicking the inner part of the semiconducting particle and some additional resistors mimicking resistances of the ITO electrode and the electrolyte are necessary for accurate modeling of the photoelectrode. The energy barrier of the Schottky junction can be characterized by its resistance and capacitance; the most convenient equivalent electric circuit of every junction contributing to the electrode is a simple RC loop circuit.[64−74] Also the semiconducting particle can be described as an RC loop.[51,52,75−77] There are, however, more complex equivalent circuits,[67,74,78−88] but a simple RC circuit reproduces the behavior of the photoelectrode sufficiently well. The simplified electric equivalent of the semiconducting photoelectrode in the studied system is shown in Figure 11.

In this model R_{ITO} stands for the resistance of the supporting ITO electrode, R_e for the resistance of the bulk electrolyte, and

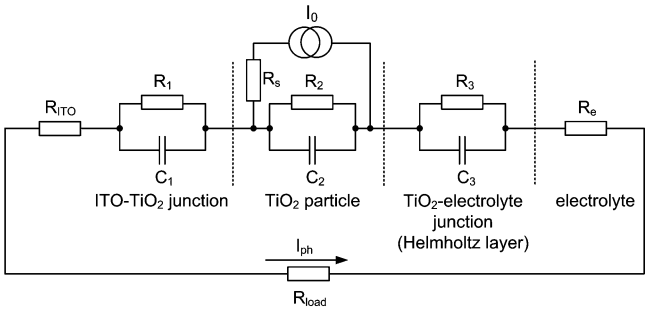

Figure 11. Equivalent electric circuit employed to describe the ITO−TiO_2−electrolyte junction.

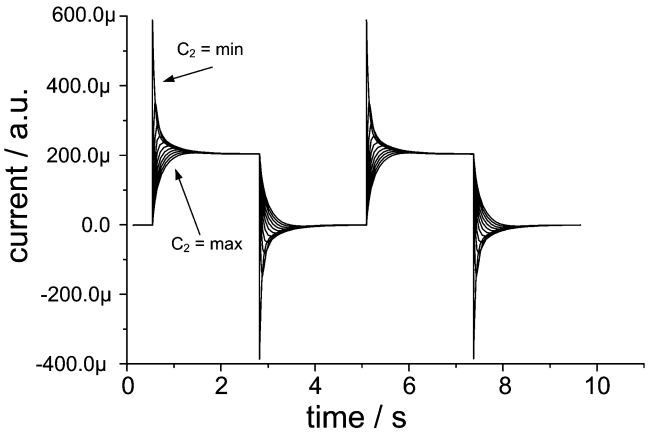

Figure 12. Simulated transient photocurrent profiles generated in the model circuit from Figure 11 for various C_2 values. See text for details.

R_{load} for the resistance of the load. I_0 represents the photocurrent square wave pulses generated at the semiconductor particle, and R_s is the resistance of the inner part of the semiconductor particle associated with the majority of carrier diffusion. The beginning of the voltage pulse corresponds to shutter opening, while the end of the pulse corresponds to shutter closure. This simple circuit can reproduce both main kinds of kinetic traces generated at the semiconductor photoelectrodes when a square wave potential is supplied to one of the terminals. To simplify the computation, $R_1 = R_2 = R_3$ and $C_1 = C_3$ were kept constant during the whole simulation, and C_2 was varied over a wide range. This choice is justified by literature examples of the strong influence of applied voltage on TiO_2 electrode capacitance.[52] The I_{ph} current flowing through R_{load} upon square wave stimulation (I_0 source) was taken as a model for the photocurrent generated by the photoelectrode upon pulsed irradiation.

When $C_2 \ll C_1$ (C_3) the current generated by the circuit has typical spiked characteristics (Figure 12) due to rapid charging of the C_1 and C_3 capacitors. When I_0 vanishes the C_1 and C_3 capacitors discharge through the load resistor yielding the reversed current pulse. With increasing C_2 capacitance the loading of the C_2 capacitor requires longer time, and the spike becomes smoother as the charging curve of the C_2 capacitor contributes more and more significantly to the overall current. At $C_2 \approx 10 \times C_1$ (C_3) the current time profile changes to a purely charge−discharge curve of the C_2 capacitor, and the spikes due to the charging of the C_1 and C_3 capacitors become invisible. Values of the C_1 and C_3 capacitors are responsible for the amplitude and shape of spikes generated at low C_2 capacitance. At very low C_1 and C_3 only current originating from charging and discharging of the C_2 capacitor can be observed. Increasing C_1 and C_3 values result in the appearance of spikes and subsequent increase of spike amplitude and prolongation of its decay time. It is consistent with increasing R_1C_1 and R_3C_3 time constants.

Real photocurrent profiles may be even more complex; as in partially reduced (or partially oxidized) material some grains behave according to one of the possible modes and some to the other. Furthermore, photoinduced electron transfer between semiconducting particles can also contribute to the net photoeletrochemical response on the electrode, and every particle−particle contact also must be regarded as a Schottky junction with its own RC characteristics.[75,89] This simple model illustrates the most important features of photocurrent generated by semiconducting photoelectrodes. The photocurrent kinetics can be switched between two limiting regimes just by changing C_2 capacitance, which corresponds to the capacitance of the semiconductor particle.

Redox changes of the surface iron species affect the properties of the surface in several ways. First of all, only the complex in the reduced form (Fe^{II}) upon deposition on the TiO_2 surface can generate the MMCT transition involving the gap surface states of the semiconductor and the HOMO of the cyanometalate anion (cf. Figure 3b). Irradiation within this band results in electron injection from the surface cyanoferrate moiety into the conduction band, which results in distinct photoactivity in visible light.

Apart from the purely electronic effects, the electrostatic influence of the surface complex on the electrons inside the semiconductor particle seems to be very important.[16] The oxidized form (containing Fe^{III}) interacts only weakly with the surface and is a relatively good electron acceptor. Therefore it should bend the valence and conduction band downward, which results in the formation of an accumulation layer, and only anodic photocurrents can be generated. Upon the electrochemical reduction of this material the surface concentration of Fe^{II} species increases, which results in formation of a depletion layer, thus facilitating photogeneration of cathodic photocurrent upon visible excitation. When the reduction is complete the semiconductor photoelectrode generates only cathodic photocurrent irrespective of irradiation wavelength, which results from formation of an inversion layer (cf. Figure 9d).

The changes of the redox state of the surface of the semiconductor particles also influence the electric properties of the ITO−semiconductor and semiconductor−electrolyte Schottky junctions. The height of the Schottky barrier depends on the charge and electron transfer properties of the surface complex. Pentacyanoferrate(II) moieties of high negative charge increase the energy of the Schottky barrier thus increasing the resistance and capacitance of the junction. This must result in significant changes in photocurrent kinetics: Transition from charging−discharging to spiked characteristics is observed during switching from anodic to cathodic regimes of photoelectrochemical activity, which is consistent with observations in an equivalent electric circuit (cf. Figures 11 and 12). Moreover it was found that the resistance and capacitance of semiconductor particles strongly depend on the electrode potential.[52] This further justifies the strong potential dependence of the kinetic behavior of surface-modified TiO_2 electrodes.

4. Conclusions and Outlook

Switching of photocurrent direction in semiconducting systems upon changes of the photoelectrode potential, incident light wavelength, or other physical stimuli is not a unique phenomenon. It has been frequently observed in the cases of organic semiconductors and composites comprised of n- and p-type semiconductors.[75,90−92] In these systems it was possible to

address optically only one distinct component of the system and thus control the photoelectric activity. The same phenomenon was observed in the cases of various nanodevices based on monolayers deposited on conducting substrates[93−97] and in photoactive liquid crystal binary systems composed of electron donor and electron acceptor mesogens.[98−100] However, many n-type semiconductor photoelectrodes can generate cathodic photocurrents at low potentials due to the formation of an inversion layer[101] or preferred reaction of the surface with electron acceptors.[102−104] The understanding of these processes is crucial for the improvement of solar cell performance[105,106] and photocatalysis. The materials described here give the possibility of photocurrent direction control by both stimuli: Changing the wavelength or the photoelectrode potential easily switches the direction of the photocurrent. These materials, however, are different from the materials of similar characteristics studied by other authors: They are not composites comprising of two types of semiconductors but are engineered uniform materials, and the photocurrent switching phenomenon is an intrinsic feature resulting from a specific electronic structure of the material. In this sense the materials described in this paper are unique.

The PEPS effect may serve as a basis for the construction of tunable light-harvesting antennae, chemical switches, and logic gates. The latter application was described previously for hexacyanoferrate and Prussian blue complexes attached to TiO_2 and CdS surfaces.[26−28] The systems presented here show different patterns of photocurrent switching, and therefore new action modes (logic functions) are available in addition to previously described systems.

Acknowledgment. This work was supported by the Polish Ministry of Education and Science (Grant Nos. PB0941/*T*08/2005/28 and PB1283/*T*09/2005/29) and by Jagiellonian University. W.M. thanks the Rector of Jagiellonian University for the fellowship.

References and Notes

(1) Kisch, H.; Macyk, W. *ChemPhysChem* **2002**, *3*, 399.
(2) Kisch, H. In *Advances in Photochemistry*; D. C. Neckers, G. von Bünau, W. S. Jenks, Eds.; John Wiley & Sons: New York, 2001; Vol. 26, p 93.
(3) Bach, U.; Lupo, D.; Comte, P.; Moser, J. E.; Weissoertel, F.; Salbeck, J.; Spreitzer, H.; Grätzel, M. *Nature* **1998**, *395*, 583.
(4) Moser, J. E.; Bonnote, P.; Grätzel, M. *Coord. Chem. Rev.* **1998**, *171*, 245.
(5) Kalyanasundaram, K.; Grätzel, M. *Coord. Chem. Rev.* **1998**, *177*, 347.
(6) Hagfeldt, A.; Grätzel, M. *Acc. Chem. Res.* **2000**, *33*, 269.
(7) Tributsch, H. *Coord. Chem. Rev.* **2004**, *248*, 1511.
(8) Beek, W. J. E.; Wienk, M. M.; Janssen, R. A. J. *J. Mater. Chem.* **2005**, *15*, 2985.
(9) Carp, O.; Huisman, C. L.; Reller, A. *Prog. Solid State Chem.* **2004**, *32*, 33.
(10) Katz, E.; Willner, I. *Angew. Chem., Int. Ed.* **2004**, *43*, 6042.
(11) Seker, F.; Meeker, K.; Kuech, T. F.; Ellis, A. B. *Chem. Rev.* **2000**, *100*, 2505.
(12) Hoffmann, M. R.; Martin, S. T.; Choi, W.; Bahnemann, D. W. *Chem. Rev.* **1995**, *95*, 69.
(13) Linsebigler, A. L.; Lu, G.; Yates Jr., J. T. *Chem. Rev.* **1995**, *95*, 735.
(14) Mills, A.; Le Hunte, S. *J. Photochem. Photobiol., A* **1997**, *108*, 1.
(15) Kisch, H.; Burgeth, G.; Macyk, W. *Adv. Inorg. Chem.* **2004**, *56*, 241.
(16) Hagfeldt, A.; Grätzel, M. *Chem. Rev.* **1995**, *95*, 49.
(17) Biancardo, M.; Bignozzi, C.; Doyle, H.; Redmond, G. *Chem. Commun.* **2005**, 3918.
(18) Will, G.; Boschloo, G.; Hoyle, R.; Rao, S. N.; Fitzmaurice, D. *J. Phys. Chem. B* **1998**, *102*, 10272.
(19) Will, G.; Sotomayor, J.; Rao, S. N.; Fitzmaurice, D. *J. Mater. Chem.* **1999**, *9*, 2297.
(20) Vieira, M.; Maçarico, A.; Fantoni, A.; Fernandes, M.; Koynov, S.; Schwartz, R. *Vacuum* **1999**, *52*, 121.
(21) Louro, P.; Vieira, M.; Fantoni, A.; Fernandes, M.; Vygranenko, Y.; Schwartz, R. *Thin Solid Films* **2003**, *427*, 196.
(22) Louro, P.; Fantoni, A.; Fernandes, M.; Maçarico, A.; Schwartz, R.; Vieira, M. *J. Non-Cryst. Solids* **2004**, *338−340*, 345.
(23) Vieira, M.; Louro, P.; Fantoni, A.; Fernandes, M. *Sens. Actuators, A* **2005**, *120*, 88.
(24) Vieira, M.; Fernandes, M.; Louro, P.; Fantoni, A.; Lavereda, G.; Nunes de Carvalho, C.; Vygranenko, Y. *Sens. Actuators, A* **2005**, *123−124*, 331.
(25) Louro, P.; Vieira, M.; Fantoni, A.; Fernandes, M.; Nunes de Carvalho, C.; Lavereda, G. *Sens. Actuators, A* **2005**, *123−124*, 326.
(26) Szaciłowski, K.; Macyk, W. *C. R. Chim.* **2006**, *9*, 315.
(27) Szaciłowski, K.; Macyk, W. *Ann. Pol. Chem. Soc.* **2004**, *4*, 768.
(28) Szaciłowski, K.; Macyk, W.; Stochel, G. *J. Am. Chem. Soc.* **2006**, *128*, 4550.
(29) Olabe, J. A. *Adv. Inorg. Chem.* **2004**, *55*, 61.
(30) Baraldo, L. M.; Forlano, P.; Parise, A. R.; Slep, L. D.; Olabe, J. A. *Coord. Chem. Rev.* **2001**, *219−221*, 881.
(31) Macartney, D. H. *Rev. Inorg. Chem.* **1988**, *9*, 101.
(32) Monzyk, M. M.; Holwerda, R. A. *Polyhedron* **1990**, *9*, 2433.
(33) Borges, S.d. S. S.; Coelho, A. L.; Moreira, I. S.; de Araújo, M. A. B. *Polyhedron* **1994**, *13*, 1015.
(34) Toma, H. E.; Takasugi, M. S. *Polyhedron* **1982**, *1*, 429.
(35) Vrachnou, E.; Vlachopoulos, N.; Grätzel, M. *J. Chem. Soc., Chem. Commun.* **1987**, 868.
(36) Vrachnou, E.; Grätzel, M.; McEvoy, A. J. *J. Electroanal. Chem.* **1989**, *258*, 193.
(37) Yang, M.; Thompson, D. W.; Meyer, G. J. *Inorg. Chem.* **2000**, *39*, 3738.
(38) Khoudiakov, M.; Parise, A. R.; Brunschwig, B. S. *J. Am. Chem. Soc.* **2003**, *125*, 4637.
(39) Yang, M.; Thompson, D. W.; Meyer, G. J. *Inorg. Chem.* **2002**, *41*, 1254.
(40) Brauer, G. *Handbook of Preparative Inorganic Chemistry*; Academic Press: London, 1963; Vol. II, p 1511.
(41) Thompson, M. A. *ArgusLab*, version 4.0; Planaria Software: Seattle, WA, 2004. http://www.arguslab.com.
(42) Thompson, M. A.; Zerner, M. C. *J. Am. Chem. Soc.* **1991**, *113*, 8210.
(43) Thompson, M. A.; Glendening, E. D.; Feller, D. *J. Phys. Chem.* **1994**, *98*, 10465.
(44) Thompson, M. A.; Schenter, G. K. *J. Phys. Chem.* **1995**, *99*, 6374.
(45) Thompson, M. A. *J. Phys. Chem.* **1996**, *100*, 14492.
(46) Casewit, C. J.; Colwell, K. S.; Rappe, A. K. *J. Am. Chem. Soc.* **1992**, *114*, 10035.
(47) Casewit, C. J.; Colwell, K. S.; Rappe, A. K. *J. Am. Chem. Soc.* **1992**, *114*, 10046.
(48) Rappe, A. K.; Goddard, W. A. *J. Phys. Chem.* **1991**, *95*, 3358.
(49) Rappe, A. K.; Colwell, K. S.; Casewit, C. J. *Inorg. Chem.* **1993**, *32*, 3438.
(50) Zerner, M. C.; Loew, G. H.; Kirchner, R. F.; Mueller-Westerhoff, U. T. *J. Am. Chem. Soc.* **1980**, *102*, 589.
(51) Ramsden, J. J.; Tóth-Boconádi, R. *J. Chem. Soc., Faraday Trans.* **1990**, *86*, 1527.
(52) Fabregat-Santiago, F.; Mora-Seró, I.; Garcia-Belmonte, G.; Bisquert, J. *J. Phys. Chem. B* **2003**, *107*, 758.
(53) Maciejowska, I.; van Eldik, R.; Stochel, G.; Stasicka, Z. *Inorg. Chem.* **1997**, *36*, 5409.
(54) Toma, H. E.; Malin, J. M.; Giesbrecht, E. *Inorg. Chem.* **1973**, *12*, 2084.
(55) Toma, H. E.; Meenochite, A. T. *Anal. Lett.* **1989**, *22*, 2105.
(56) Toma, H. E.; Oliveira, D.; Meenochite, A. T. *Talanta* **1988**, *35*, 323.
(57) Norris, P. R.; Harper, P. L. S.; Pratt, J. M. *J. Chem. Soc., Dalton Trans.* **1997**, 2505.
(58) De Angelis, F.; Tilocca, A.; Selloni, A. *J. Am. Chem. Soc.* **2004**, *126*, 15024.
(59) Sawyer, D. T.; Valentine, J. S. *Acc. Chem. Res.* **1981**, *14*, 393.
(60) Stanbury, D. M. *Adv. Inorg. Chem.* **1989**, *33*, 69.
(61) Bard, A. J.; Bocarsly, A. B.; Fan, F.-R. F.; Walton, E. G.; Wrighton, M. S. *J. Am. Chem. Soc.* **1980**, *102*, 3671.
(62) Shiga, A.; Tsujiko, A.; Ide, T.; Yae, S.; Nakato, Y. *J. Phys. Chem. B* **1998**, *102*, 6049.
(63) Sparnaay, M. J. *The Electrical Double Layer*; Pergamon Press: Oxford, U.K., 1972.
(64) Metikoš-Huković, M.; Omanović, S.; Jukić, A. *Electrochim. Acta* **1999**, *45*, 977.
(65) Sharma, G. D.; Sharma, S. K.; Roy, M. S. *Thin Solid Films* **2004**, *468*, 208.

(66) Aroutiounian, V. M.; Arakelyan, V. M.; Shahnazaryan, G. E.; Stepanyan, G. M.; Turner, J. A.; Kocha, S. S. *Electrochim. Acta* **2000**, *45*, 1999.
(67) Gomes, W. P.; Vanmaekelbergh, D. *Electrochim. Acta* **1996**, *41*, 967.
(68) Sharma, G. D.; Sharma, S.; Roy, M. S. *Mater. Sci. Eng., B* **2004**, *110*, 135.
(69) Oliva, F. Y.; Avalle, L. B.; Macagno, A. V.; De Pauli, C. P. *Biophys. Chem.* **2001**, *91*, 141.
(70) Zhang, D.; Liu, Z.; Yue, H.; Yao, K. *Physica B* **2004**, *334*, 265.
(71) Simons, W.; Hubin, A.; Vereechen, J. *Electrochim. Acta* **1999**, *44*, 4373.
(72) Avalle, L. B.; Cámara, O. R.; Oliva, F. Y. *J. Electroanal. Chem.* **2005**, *585*, 281.
(73) Aroutiounian, V. M.; Arakelyan, V. M.; Shahnazaryan, G. E.; Stepanyan, G. M.; Turner, J. A.; Khaselev, O. *Int. J. Hydrogen Energy* **2002**, *27*, 33.
(74) Aroutiounian, V. M.; Arakelyan, V. M.; Shahnazaryan, G. E.; Stepanyan, G. M.; Khachaturyan, E. A.; Turner, J. A. *C. R. Chim.* **2006**, *9*, 325.
(75) Rammelt, U.; Hebestreit, N.; Fikus, A.; Plieth, W. *Electrochim. Acta* **2001**, *46*, 2363.
(76) Peter, L. M. *Chem. Rev.* **1990**, *90*, 753.
(77) Ritchie, I. M.; Bailey, S.; Woods, R. *Adv. Colloid Surf. Sci.* **1999**, *80*, 183.
(78) Talapin, D. V.; Sviridov, D. V.; Kulak, A. I. *J. Electroanal. Chem.* **2000**, *489*, 28.
(79) Ponomarev, E. A.; Peter, L. M. *J. Electroanal. Chem.* **1995**, *396*, 219.
(80) Reynolds, S.; Main, C.; Rose, M. J. *J. Non-Cryst. Solids* **1998**, *227*−*230*, 233.
(81) Dolata, M.; Kedzierzawski, P.; Augustynski, J. *Electrochim. Acta* **1996**, *41*, 1287.
(82) Rajeshwar, K. In *Encyclopedia of Electrochemistry*; Bard, A. J., Stratmann, M., Licht, S., Eds.; Wiley-VCH: Weinheim, Germany, 2002; Vol. VI, p 1.
(83) Hens, Z. *J. Chem. Phys. B* **1999**, *103*, 122.
(84) Hens, Z.; Gomes, W. P. *J. Chem. Phys. B* **1997**, *101*, 5814.
(85) Hens, Z.; Gomes, W. P. *J. Phys. Chem. B* **1999**, *103*, 130.
(86) Pyun, S.-I.; Hyun, S.-M. *Int. J. Hydrogen Energy* **1995**, *20*, 71.
(87) Vanmaekelbergh, D. *Electrochim. Acta* **1997**, *42*, 1121.
(88) Vanmaekelbergh, D. *Electrochim. Acta* **1997**, *42*, 1135.
(89) Bay, L.; West, K. *Sol. Energy Mater. Sol. Cells* **2005**, *87*, 613.
(90) de Tacconi, N.; Chenthamarakshan, C. R.; Rajeshwar, K.; Tacconi, E. J. *J. Phys. Chem. B* **2005**, *109*, 11953.
(91) Vu, Q.-T.; Pavlik, M.; Hebestreit, N.; Rammelt, U.; Plieth, W.; Pfleger, J. *React. Funct. Polym.* **2005**, *65*, 69.
(92) Signerski, R.; Koœcielska, B. *Opt. Mater.* **2005**, *27*, 1480.
(93) Yasutomi, S.; Morita, T.; Imanishi, Y.; Kimura, S. *Science* **2004**, *304*, 1944.
(94) Nitahara, S.; Tasaki, N.; Akiyama, T.; Yamada, S. *Thin Solid Films* **2006**, *499*, 354.
(95) Yasutomi, S.; Morita, T.; Kimura, S. *J. Am. Chem. Soc.* **2005**, *127*, 14564.
(96) Matsui, J.; Mitsuishi, M.; Aoki, A.; Miyashita, T. *J. Am. Chem. Soc.* **2004**, *126*, 3708.
(97) Gill, R.; Patolsky, F.; Katz, E.; Willner, I. *Angew. Chem., Int. Ed.* **2005**, *44*, 4554.
(98) Donovan, K. J.; Scott, K.; Somerton, M.; Preece, J.; Manickam, M. *Chem. Phys.* **2006**, *322*, 471.
(99) Rybak, A.; Pfleger, J.; Jung, J.; Pavlik, M.; Glowacki, I.; Ulanski, J.; Tomovic, Z.; Müllen, K.; Geerts, Y. *Synth. Met.* **2006**, *156*, 302.
(100) Han, S.-H.; Yoshida, H.; Iwahori, F.; Abe, J. *Sci. Technol. Adv. Mater.* **2006**, *7*, 62.
(101) Dare-Edwards, M. P.; Goodenough, J. B.; Hamnett, A.; Travellick, P. R. *J. Chem. Soc., Faraday Trans. 1* **1983**, *79*, 2027.
(102) Tsujiko, A.; Itoh, H.; Kisumi, T.; Shiga, A.; Murakoshi, K.; Nakato, Y. *J. Phys. Chem. B* **2002**, *106*, 5878.
(103) Lindgren, T.; Lu, J.; Hoel, A.; Grandqvist, C. C.; Torres, G. R.; Lindquist, S.-E. *Sol. Energy Mater. Sol. Cells* **2004**, *84*, 145.
(104) Lana-Villareal, T.; Gómez, R. *Chem. Phys. Lett.* **2005**, *414*, 489.
(105) Tachibana, Y.; Hara, K.; Takano, S.; Sayama, K.; Arakawa, H. *Chem. Phys. Lett.* **2002**, *364*, 297.
(106) Agostinelli, G.; Dunlop, E. D. *Thin Solid Films* **2003**, *431*−*432*, 448.